Fresnel approximations for acoustic fields of rectangularly symmetric sources

T. Douglas Mast[a)]
Department of Biomedical Engineering, University of Cincinnati, Cincinnati, Ohio 45267-0586

(Received 8 December 2006; revised 19 March 2007; accepted 20 March 2007)

A general approach is presented for determining the acoustic fields of rectangularly symmetric, baffled, time-harmonic sources under the Fresnel approximation. This approach is applicable to a variety of separable source configurations, including uniform, exponential, Gaussian, sinusoidal, and error function surface velocity distributions, with and without focusing in either surface dimension. In each case, the radiated field is given by a formula similar to that for a uniform rectangular source, except for additional scaling of wave number and azimuthal distance parameters. The expressions presented are generalized to three different Fresnel approximations that correspond, respectively, to diffracted plane waves, diffracted spherical waves, or diffracted cylindrical waves. Numerical results, for several source geometries relevant to ultrasonic applications, show that these expressions accurately depict the radiated pressure fields, except for points very near the radiating aperture. Highest accuracy near the source is obtained by choice of the Fresnel approximation most suited to the source geometry, while the highest accuracy far from the source is obtained by the approximation corresponding to diffracted spherical waves. The methods are suitable for volumetric computations of acoustic fields including focusing, apodization, and attenuation effects. © *2007 Acoustical Society of America.* [DOI: 10.1121/1.2726252]

PACS number(s): 43.20.Rz, 43.20.El [JJM] Pages: 3311–3322

I. INTRODUCTION

Radiated fields from rectangularly symmetric apertures, and from arrays of rectangularly symmetric elements, are important to many acoustic applications. In particular, certain ultrasound applications require computation of diffracted pressure fields over a large number of spatial points in two or three dimensions. These include modeling of ultrasound-induced heating for simulation of ultrasound therapy,[1–3] simulation of ultrasound imaging systems,[4–7] and compensation for diffraction effects in quantitative scattering measurements.[8–10] In such problems, individual elements of ultrasonic linear arrays, phased arrays, or two-dimensional arrays can be modeled as baffled rectangular sources, each of which may be unfocused, or focused in one or both dimensions, with possibly different focal lengths in each direction. The position-dependent surface velocity of such an array element may be approximately uniform over the entire rectangular aperture, or may be spatially varying (e.g., apodized to reduce beam sidelobes).[11]

A number of numerical methods are available for computation of ultrasonic fields from rectangular sources. Fields can be computed accurately using the angular spectrum method,[12,13] in which the Rayleigh integral is numerically evaluated by fast Fourier transform operations. Several numerically exact methods have been based on numerical integration of the aperture's space-time impulse response[14] for uniform, flat[15–18] or spherically focused[19] rectangular sources. A more general and computationally intensive method employs numerical evaluation of the two-dimensional Rayleigh integral[20] or the impulse response integral[6,21] by dividing a radiating surface into many small canonical elements. Recent work using the impulse-response method has included a method for rapid computation of the exact time-harmonic field for flat rectangular sources[18] and an approximate method for cylindrically focused sources.[22]

Approximate methods for computation of ultrasonic fields include several based on the Fresnel approximation, in which the phase of a wave front emanating from the radiating surface is replaced within the Rayleigh integral by a binomial-series expansion, truncated at second (quadratic) order.[23] In contrast to available numerical methods, the Fresnel approximation allows simple, analytic solutions for diffracted pressure fields to be obtained for rectangularly symmetric sources,[24] including apodized radiators for which "exact" numerical methods such as the impulse response approach may not be tractable.[25] In addition, the Fresnel approximation forms the basis for efficient numerical methods such as Gaussian beam expansions.[26–28] Analytic solutions obtained from the Fresnel approximation are desirable because they are amenable to further analysis, and can provide physical insight.

Analytic solutions for rectangularly symmetric apertures, under the Fresnel approximation, have previously been presented for a uniform, flat rectangular aperture[24] as well as for unfocused rectangularly symmetric apertures with several apodization patterns.[25] Szabo has pointed out that under the Fresnel approximation, the effect of focusing is similar to a scaling of the field of unfocused transducers.[11] Still, several investigators have implied that simple analytic solutions for Fresnel diffraction from focused rectangular transducers are not tractable outside the focal plane.[4,8,29,30]

[a)]Electronic mail: doug.mast@uc.edu

In this paper, analytic solutions are derived for the acoustic fields of a large class of rectangularly symmetric apertures under the Fresnel approximation. The general approach derived here for solution of the Rayleigh integral is valid for separable surface velocity distributions under three variations of the Fresnel approximation, respectively representing diffracted plane, spherical, and cylindrical waves. The result of this approach is a single, compact analytic formula for the fields of several focused and unfocused rectangularly symmetric apertures with various apodizations, all of which take a similar functional form except for shifting and scaling of wave number and azimuthal coordinates. Numerical results obtained from this simple approach indicate that each of the Fresnel approximations considered provides different numerical accuracy, dependent on the region of interest. An appropriate choice of Fresnel approximation, based on the aperture geometry, allows accurate field computations to be made over a wide region including the geometric near field. In addition, the simple form of the derived solutions, written in terms of the complex error function or Fresnel integral, facilitates further mathematical analysis of radiated acoustic fields. Thus, the methods introduced here should be useful for a wide variety of ultrasound applications that require detailed knowledge of the ultrasound field structure.

II. THEORY

In the following, an analytic approach is given that provides closed-form solutions of the Rayleigh integral for a variety of rectangularly symmetric apertures, under the Fresnel approximation. Four related variants of the Fresnel approximation are presented, which represent the radiated acoustic field respectively as a diffracted plane wave, a diffracted spherical wave, or diffracted cylindrical waves centered on either axis of symmetry. These four Fresnel approximations are generalized into a common form. Compact analytic solutions for this generalized Fresnel approximation are then derived for rectangularly symmetric apertures with uniform, exponential, sinusoidal, Gaussian, or error-function apodization, both for unfocused and focused apertures. In all cases, the pressure field is specified by a formula similar to that for a uniform, unfocused rectangular aperture,[24] but with complex, position-dependent shifting and scaling of the acoustic wave number and azimuthal distance coordinates.

A. General solution

The problem geometry considered here is the classic baffled piston, sketched in Fig. 1. A planar source at $z=0$, placed within an infinite rigid baffle, oscillates with time-harmonic surface velocity $u(x_0,y_0)=u_0A(x_0,y_0)e^{-i\omega t}$. For such a source, the resulting linear acoustic field pressure at any point in a homogeneous medium is given exactly by the Rayleigh integral:[31]

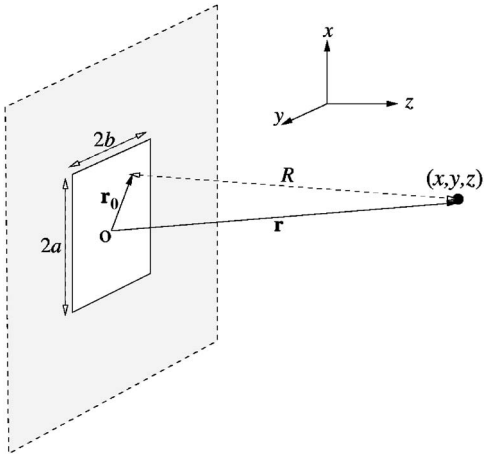

FIG. 1. Problem geometry. A rectangularly symmetric source with dimensions $2a$ in the x direction and $2b$ in the y direction oscillates within an infinite rigid baffle. The origin $\mathbf{o}$ of the coordinate system is at the aperture center. The pressure field at a field point $\mathbf{r}=(x,y,z)$ is given by the Rayleigh integral over the surface coordinate $\mathbf{r}_0=(x_0,y_0)$, with an integrand dependent on the distance $R=|\mathbf{r}-\mathbf{r}_0|$.

$$p(\mathbf{r},t)=-\frac{ik}{2\pi}\rho c u_0 e^{-i\omega t}\int_{-\infty}^{\infty}\int_{-\infty}^{\infty}A(x_0,y_0)\frac{e^{ik|\mathbf{r}-\mathbf{r}_0|}}{|\mathbf{r}-\mathbf{r}_0|}dx_0dy_0, \tag{1}$$

where ρ is the medium mass density, c is the speed of sound, k is the wave number ω/c, and the distance between a field point (x,y,z) and a surface point (x_0,y_0) is

$$|\mathbf{r}-\mathbf{r}_0|=\sqrt{(x-x_0)^2+(y-y_0)^2+z^2}. \tag{2}$$

This expression for the pressure field is also valid for attenuating media, in which case k is complex with $\mathrm{Im}[k]>0$. In the derivations given here, the time-dependent factor $e^{-i\omega t}$ will be suppressed and the nominal surface pressure $p_0=\rho c u_0$ will be assumed equal to unity.

The usual Fresnel approximation[23,24] starts with the assumption that

$$(x-x_0)^2+(y-y_0)^2 \ll z^2$$

for the surface points that contribute significantly to the pressure at a field point. This assumption, which is not required to hold for all points on the radiating surface, is consistent with the principle of stationary phase.[23] In this case, the distance $|\mathbf{r}-\mathbf{r}_0|$ can be approximated by the leading terms of its binomial expansion,

$$|\mathbf{r}-\mathbf{r}_0|\approx z+[(x-x_0)^2+(y-y_0)^2]/(2z), \tag{3}$$

so that the exponential term of Eq. (1) can be approximated as

$$\frac{e^{ik|\mathbf{r}-\mathbf{r}_0|}}{|\mathbf{r}-\mathbf{r}_0|}\approx\frac{e^{ikz}}{z}e^{ik[(x-x_0)^2+(y-y_0)^2]/(2z)}. \tag{4}$$

The pressure field given by the Rayleigh integral (1) is thus approximated as a plane wave multiplied by an integral diffraction term. For this reason, the Fresnel approximation of Eq. (4) is particularly useful for large sources in their acoustic near field and within the paraxial region.

Other implementations of the Fresnel approximation result from alternate binomial expansions of the distance $|\mathbf{r}-\mathbf{r}_0|$ into a position-independent distance plus a quadratic, position-dependent perturbation term, similar to Eq. (3). The result in each case is an expression of the radiated field as a simple geometric wave field (e.g., a plane, spherical, or cylindrical wave) multiplied by an integral diffraction term. In a given problem, optimal choice for the form of this expansion depends on the source geometry as well as the field position, as demonstrated by the numerical results presented later in this paper.

One alternate Fresnel approximation is more appropriate for small acoustic sources, such as rectangular elements of a two-dimensional ultrasonic array. For such sources, an appropriate scaling is based on the assumption

$$x_0^2 + y_0^2 - 2xx_0 - 2yy_0 \ll r^2,$$

where $r=\sqrt{x^2+y^2+z^2}$. This assumption is valid wherever the distance from the source center to the field point is much larger than any source dimension, so that it also applies in the geometric far field of any acoustic source. The most appropriate Fresnel approximation for this case represents a diffracted spherically spreading wave, so that the integrand of the Rayleigh integral (1) is approximated as

$$\frac{e^{ik|\mathbf{r}-\mathbf{r}_0|}}{|\mathbf{r}-\mathbf{r}_0|} \approx \frac{e^{ikr}}{r} e^{ik(x_0^2+y_0^2-2xx_0-2yy_0)/(2r)}. \tag{5}$$

A third approximation is useful for the common source configuration where an acoustic source is small in one dimension and large in the other dimension, such as an element of a typical linear or phased ultrasonic array. In the acoustic near field of such a transducer, one may assume that

$$(x-x_0)^2 + y_0^2 - 2yy_0 \ll y^2 + z^2$$

for source points that significantly contribute to the pressure field, where x is the direction of the longer element dimension (elevation or height) and y is the direction of the shorter element dimension (azimuth or pitch). In this case, an approximation analogous to Eqs. (4) and (5) is

$$\frac{e^{ik|\mathbf{r}-\mathbf{r}_0|}}{|\mathbf{r}-\mathbf{r}_0|} \approx \frac{e^{ikw_y}}{w_y} e^{ik[(x-x_0)^2+y_0^2-2yy_0]/(2w_y)}, \tag{6}$$

where $w_y \equiv \sqrt{y^2+z^2}$. This represents a diffracted yz-plane cylindrically spreading wave, centered on the long axis of the source.

Similarly, for a source that is much larger in the y dimension than the x dimension, one may make the approximation

$$\frac{e^{ik|\mathbf{r}-\mathbf{r}_0|}}{|\mathbf{r}-\mathbf{r}_0|} \approx \frac{e^{ikw_x}}{w_x} e^{ik[(y-y_0)^2+x_0^2-2xx_0]/(2w_x)}, \tag{7}$$

where $w_x \equiv \sqrt{x^2+z^2}$. This represents a diffracted wave cylindrically spreading in the xz plane, centered on the long axis of the radiating aperture.

The Rayleigh integral can be solved in a similar manner for any of these Fresnel approximations. For convenience, the four approximations are generalized here so that analytic expressions derived for the pressure field are valid under any of these approximations. To achieve this, a distance ζ is defined as the position-independent portion of any binomial expansion for $|\mathbf{r}-\mathbf{r}_0|$, e.g., $\zeta=z$ for Eq. (4). Given this definition, Eqs. (4)–(7) can be summarized by the compact expression

$$\frac{e^{ik|\mathbf{r}-\mathbf{r}_0|}}{|\mathbf{r}-\mathbf{r}_0|} \approx \frac{e^{ik(r^2+\zeta^2)/(2\zeta)}}{\zeta} e^{ik(x_0^2+y_0^2-2xx_0-2yy_0)/(2\zeta)}, \tag{8}$$

where one may choose $\zeta=z$ to represent the field as a diffracted plane wave (4), $\zeta=r$ for a spherically spreading wave (5), or $\zeta=w_y$ (6) or $\zeta=w_x$ (7) for cylindrically spreading waves. In each case, the coordinate ζ can be regarded as the nominal propagation distance from the source to a field point.

For sources with a separable surface velocity distribution such that $A(x_0,y_0)=A_x(x_0)A_y(y_0)$, the Rayleigh integral (1) can be written for any of the Fresnel approximations represented by Eq. (8) as

$$p(\mathbf{r}) = -\frac{ike^{ik(r^2+\zeta^2)/(2\zeta)}}{2\pi\zeta} \int_{-\infty}^{\infty} A_x(x_0) e^{ik(x_0^2-2xx_0)/(2\zeta)} dx_0 \times \int_{-\infty}^{\infty} A_y(y_0) e^{ik(y_0^2-2yy_0)/(2\zeta)} dy_0, \tag{9}$$

where the harmonic time dependence has been suppressed and the surface pressure $\rho c u_0$ is taken without loss of generality to be unity. Thus, the Fresnel approximation can allow the pressure field to be represented by two multiplicative integral terms, one depending on each of the azimuthal coordinates x and y.

Many surface velocity distributions of practical interest can be represented by simple exponential functions that are conveniently expressed in the form

$$A_x(x_0) = e^{\xi_2 x_0^2 + \xi_1 x_0}, \quad |x| < a,$$

$$A_y(y_0) = e^{\eta_2 y_0^2 + \eta_1 y_0}, \quad |y| < b, \tag{10}$$

where ξ_1, ξ_2, η_1, and η_2 may have both real parts, representing amplitude weightings such as apodization, and imaginary parts, representing phase weightings such as used for focusing. Source velocity distributions that can be represented in this form include focused and unfocused uniform, exponentially apodized, Gaussian, and sinusoidally varying apertures, all of which are specifically considered in the following section.

For surface velocity profiles of the form described by Eq. (10), the pressure field defined by Eq. (9) can be then written as

$$p(\mathbf{r}) = -\frac{ike^{ik(r^2+\zeta^2)/(2\zeta)}}{2\pi\zeta} \int_{-a}^{a} e^{i(\tilde{k}_x x_0^2 - 2k\tilde{x}x_0)/(2\zeta)} dx_0 \times \int_{-b}^{b} e^{i(\tilde{k}_y y_0^2 - 2k\tilde{y}y_0)/(2\zeta)} dy_0, \tag{11}$$

where

$$\tilde{k}_x \equiv k - 2i\xi_2\zeta, \quad \tilde{k}_y \equiv k - 2i\eta_2\zeta,$$

TABLE I. Summary of the four instances of the Fresnel approximation considered here, including the defining coordinates ζ, regions of greatest applicability, and forms of the multiplicative term $\Phi(\mathbf{r},\zeta)$.

Approximation	Most useful region	$\Phi(\mathbf{r},\zeta)$
$\zeta=z$ (diffracted plane wave)	$\lvert x\rvert\leqslant a$, $\lvert y\rvert\leqslant b$	$e^{ikz}e^{ik[x^2+y^2-k(\tilde{x}^2/\tilde{k}_x+\tilde{y}^2/\tilde{k}_y)]/(2z)}$
$\zeta=r$ (diffracted spherical wave)	$r\geqslant\sqrt{a^2+b^2}$	$e^{ikr}e^{-ik^2(\tilde{x}^2/\tilde{k}_x+\tilde{y}^2/\tilde{k}_y)/(2r)}$
$\zeta=w_y=\sqrt{y^2+z^2}$ (diffracted yz-plane cylindrical wave)	$\lvert x\rvert\leqslant a$	$e^{ikw_y}e^{ik[x^2-k(\tilde{x}^2/\tilde{k}_x+\tilde{y}^2/\tilde{k}_y)]/(2w_y)}$
$\zeta=w_x=\sqrt{x^2+z^2}$ (diffracted xz-plane cylindrical wave)	$\lvert y\rvert\leqslant b$	$e^{ikw_x}e^{ik[y^2-k(\tilde{x}^2/\tilde{k}_x+\tilde{y}^2/\tilde{k}_y)]/(2w_x)}$

$$\tilde{x}\equiv x+i\frac{\xi_1\zeta}{k},\quad \tilde{y}\equiv y+i\frac{\eta_1\zeta}{k}. \tag{12}$$

Comparison with Eq. (9) indicates that Eq. (11) represents the pressure fields for a wide variety of rectangularly symmetric sources in terms of the field of an unfocused, unapodized rectangular source, with the introduction of scaled and shifted wave numbers $\tilde{k}_x$, $\tilde{k}_y$ and distances $\tilde{x}$, $\tilde{y}$. In general, these scaled and shifted parameters are complex and position-dependent.

For any source velocity distribution represented by Eq. (10), the resulting pressure field under any of the approximations (4)–(7) is given by Eq. (11). Solutions to the integrals appearing in Eq. (11) are obtained by completing the square in each exponent and applying definitions of the complex error function or the complex Fresnel integral. This results in closed-form expressions for the pressure field under the Fresnel approximation:

$$\begin{aligned}p(\mathbf{r}) &= \frac{k\Phi(\mathbf{r},\zeta)}{4\sqrt{\tilde{k}_x}\sqrt{\tilde{k}_y}}\left(\operatorname{erf}\left[\frac{k\tilde{x}+\tilde{k}_x a}{\sqrt{2i}\sqrt{\tilde{k}_x\zeta}}\right]-\operatorname{erf}\left[\frac{k\tilde{x}-\tilde{k}_x a}{\sqrt{2i}\sqrt{\tilde{k}_x\zeta}}\right]\right)\\ &\times\left(\operatorname{erf}\left[\frac{k\tilde{y}+\tilde{k}_y b}{\sqrt{2i}\sqrt{\tilde{k}_y\zeta}}\right]-\operatorname{erf}\left[\frac{k\tilde{y}-\tilde{k}_y b}{\sqrt{2i}\sqrt{\tilde{k}_y\zeta}}\right]\right)\\ &= -\frac{ik\Phi(\mathbf{r},\zeta)}{2\sqrt{\tilde{k}_x}\sqrt{\tilde{k}_y}}\left(\mathbf{F}\left[\frac{k\tilde{x}+\tilde{k}_x a}{\sqrt{\pi}\sqrt{\tilde{k}_x\zeta}}\right]-\mathbf{F}\left[\frac{k\tilde{x}-\tilde{k}_x a}{\sqrt{\pi}\sqrt{\tilde{k}_x\zeta}}\right]\right)\\ &\times\left(\mathbf{F}\left[\frac{k\tilde{y}+\tilde{k}_y b}{\sqrt{\pi}\sqrt{\tilde{k}_y\zeta}}\right]-\mathbf{F}\left[\frac{k\tilde{y}-\tilde{k}_y b}{\sqrt{\pi}\sqrt{\tilde{k}_y\zeta}}\right]\right),\end{aligned} \tag{13}$$

where the multiplicative term $\Phi(\mathbf{r},\zeta)$ is defined as

$$\Phi(\mathbf{r},\zeta)=e^{i[k(r^2+\zeta^2)-k^2(\tilde{x}^2/\tilde{k}_x+\tilde{y}^2/\tilde{k}_y)]/(2\zeta)}. \tag{14}$$

In Eq. (13), erf denotes the error function[32] and $\mathbf{F}$ denotes the complex Fresnel integral

$$\mathbf{F}(\zeta)=C(\zeta)+iS(\zeta)\equiv\int_0^\zeta e^{i\pi u^2/2}du. \tag{15}$$

These two functions are related by the identity[32]

$$\mathbf{F}(\zeta)=\sqrt{\frac{i}{2}}\operatorname{erf}\left(\sqrt{\frac{\pi}{2i}}\zeta\right). \tag{16}$$

Both of these functions have been analyzed in depth[32] and can be computed efficiently using series expansions, rational approximations, or other available numerical methods, similar to other tabulated special functions.[33,34]

Specific expressions for the factor $\Phi(\mathbf{r},\zeta)$ are given in Table I for the cases $\zeta=z$, $\zeta=r$, $\zeta=w_x$, and $\zeta=w_y$ corresponding to the four Fresnel approximations described earlier. Table I also lists the regions where each approximation is most likely to be valid, based on simple geometric considerations borne out by the numerical results presented in Sec. III. Notable is that, although $\Phi(\mathbf{r},\zeta)$ takes the form of a complex exponential function, this factor does not have unity magnitude except in special cases (e.g., an unapodized rectangular aperture in a lossless medium).

The general expressions given by Eq. (13) for the pressure field have functional form equivalent to previous results for the field of uniform rectangular sources under the Fresnel approximation,[24,25] but with scaled and shifted variables according to Eq. (12). Thus, the same computational and analytic formulas can be applied, with modification only to the independent variables, to any unfocused or focused radiator described by Eq. (10). Solutions for specific apertures are detailed in the following section.

B. Pressure fields for specific apertures

Pressure fields for a number of practically important amplitude distributions can be obtained directly from the general result of Eq. (13), using scaled wave numbers $\tilde{k}_x$, $\tilde{k}_y$ and scaled coordinates $\tilde{x}$, $\tilde{y}$ defined by Eq. (12). Table II lists values of the scaled wave number $\tilde{k}_x$ and the scaled distance $\tilde{x}$ for several apertures of the form given by Eq. (10), including unfocused and focused rectangular, sinusoidal, and Gaussian distributions, as well as the general quadratic exponential function that encompasses all these cases.

The scaled wave number and distance parameters listed in Table II are in general complex. In the case of a Gaussian aperture, the scaled wave number $\tilde{k}_x$ has a positive imaginary part, similar to the positive imaginary part of the physical

TABLE II. Complex apodization functions $A_x(x_0)$, scaled wave numbers $\tilde{k}_x$; and scaled azimuthal distances $\tilde{x}$ for four unfocused and focused apertures.

Aperture type	$A_x(x_0)$	$\tilde{k}_x$	$\tilde{x}$
Quadratic exponential	$e^{\beta_2 x_0^2+\beta_1 x_0}$	$k-2i\beta_2\zeta$	$x+i\frac{\beta_1\zeta}{k}$
Rectangular	1	k	x
Sinusoidal	$e^{i\kappa x_0}$	k	$x-\frac{\kappa\zeta}{k}$
Gaussian	$e^{-x_0^2/(2\sigma_x^2)}$	$k+i\frac{\zeta}{\sigma_x^2}$	x
Focused quadratic exponential	$e^{\beta_2 x_0^2+\beta_1 x_0 e^{-ikx_0^2/(2F_x)}}$	$k\left(1-\frac{\zeta}{F_x}\right)-2i\beta_2\zeta$	$x+i\frac{\beta_1\zeta}{k}$
Focused rectangular	$e^{-ikx_0^2/(2F_x)}$	$k\left(1-\frac{\zeta}{F_x}\right)$	x
Focused sinusoidal	$e^{i\kappa x_0}e^{-ikx_0^2/(2F_x)}$	$k\left(1-\frac{\zeta}{F_x}\right)$	$x-\frac{\kappa\zeta}{k}$
Focused Gaussian	$e^{-x_0^2/(2\sigma_x^2)}e^{-ikx_0^2/(2F_x)}$	$k\left(1-\frac{\zeta}{F_x}\right)+\frac{i\zeta}{\sigma_x^2}$	x

wave number k in an attenuating medium. This is consistent with the spatial smoothing of the diffraction pattern caused by amplitude apodization, which is qualitatively similar to the smoothing observed for uniform apertures in an attenuating medium.[35] Similarly, an exponential amplitude term of the form $A_x(x_0)=e^{\beta_1 x_0}$ results in a positive imaginary part for the scaled azimuthal coordinate $\tilde{x}$, suggesting a corollary with inhomogeneous plane waves, in which the pressure amplitude varies exponentially with the azimuthal position.[36] However, the general solution of Eq. (13) also depends on the unscaled wave number k and unscaled azimuthal coordinates x and y, so that precise physical interpretation of the scaled wave numbers $\tilde{k}_x$, $\tilde{k}_y$ and coordinates $\tilde{x}$, $\tilde{y}$ is not straightforward.

Focusing at a distance F_x is represented in Table II by phase factors of the form

$$A_x(x_0)=e^{-ikF_x(1-\sqrt{1-x_0^2/F_x^2})}\approx e^{-ikx_0^2/(2F_x)},$$

$$A_y(y_0)=e^{-ikF_y(1-\sqrt{1-y_0^2/F_y^2})}\approx e^{-iky_0^2/(2F_y)}, \tag{17}$$

where F_x and F_y are focal lengths for the elevation and azimuth directions, respectively. Thus, the phasing associated with geometric focusing at radii F_x or F_y is approximated quadratically, consistent with the quadratic truncation of the binomial series that results in the Fresnel approximations (4)–(7).

To obtain the time-harmonic pressure field for any focused or unfocused aperture of a form listed in Table II, the coordinates ζ, $\tilde{k}_x$, $\tilde{k}_y$, $\tilde{x}$, and $\tilde{y}$ are specified based on Tables I and II, and the pressure field is then given in terms of the complex error function or the complex Fresnel integral by Eq. (13). For the special case of unfocused rectangular apertures, pressure fields obtained by this method are analogous to results previously reported in the literature,[24,25] but are more general because they are applicable to any of the Fresnel approximations (4)–(7). In Sec. III, it is shown that an appropriate choice of ζ can substantially improve the accuracy of pressure computations in the nearfield.

The definitions given in Table II for the sinusoidal aperture can be employed with Eq. (13) to compute pressure fields for a number of apodizations of interest. For example, fields due to truncated-cosine, Hanning, or Hamming-apodized sources can be obtained by appropriately superposing the fields from sinusoidal apertures with spatial frequencies κ, $-\kappa$, and 0. As a specific example, the radiated field can be computed for a velocity distribution

$$A(x_0,y_0)=A_x(x_0)A_y(y_0)$$

with

$$A_x(x_0)=\cos\left(\frac{\pi}{2a}x_0\right),\quad |x|<a,$$

$$A_y(y_0)=\cos\left(\frac{\pi}{2b}y_0\right),\quad |y|<b, \tag{18}$$

which corresponds to the lowest-order vibration mode of a rectangular membrane and is similar to the "simply-supported piston" distribution used by Greenspan.[37] Using the complex representation of the cosine, the radiated pressure for this velocity distribution under the Fresnel approximation is found to be

$$p(\mathbf{r})=\frac{1}{4}\left[p_s\left(\mathbf{r},\frac{\pi}{2a},\frac{\pi}{2b}\right)+p_s\left(\mathbf{r},\frac{\pi}{2a},-\frac{\pi}{2b}\right)+p_s\left(\mathbf{r},-\frac{\pi}{2a},\frac{\pi}{2b}\right)+p_s\left(\mathbf{r},-\frac{\pi}{2a},-\frac{\pi}{2b}\right)\right], \tag{19}$$

where $p_s(\mathbf{r},\kappa_x,\kappa_y)$ is the pressure field defined by Eq. (13) and Table II for a sinusoidal velocity distribution with spatial frequencies κ_x and κ_y.

Similarly, fields of more complex, general asymmetric apertures can be obtained by representing their surface velocity distribution as a spatial-frequency Fourier series and superposing the fields computed for each Fourier component. In the resulting summation, the superposed field for each spatial-frequency component would be weighted by the complex Fourier coefficient of the surface velocity distribution for that spatial frequency.

For the source velocity distributions listed in Table II, the pressure field defined by Eq. (11) simplifies further in several limiting cases. One such case occurs when the quadratic terms in the exponential arguments of Eq. (11) can be neglected. This requires either that $\zeta \gg \tilde{k}_x x_0^2$ and $\zeta \gg \tilde{k}_y y_0^2$ (the far field or Fraunhofer approximation), or $\tilde{k}_x=\tilde{k}_y=0$, as for

certain focused apertures when the coordinate ζ is equal to the focal distance. For the Fresnel approximation obtained by setting $\zeta=z$, the latter case results in a pressure distribution in the focal plane that is equivalent to a scaled far-field pattern of the same source distribution.[11,23] For either of these conditions, the pressure field resulting from Eq. (9) becomes

$$p(\mathbf{r}) \to -\frac{2ikab}{\pi}\frac{e^{ik(r^2+\zeta^2)/(2\zeta)}}{\zeta}\mathrm{sinc}\left(\frac{ka\tilde{x}}{\zeta}\right)\mathrm{sinc}\left(\frac{kb\tilde{y}}{\zeta}\right), \quad (20)$$

where $\mathrm{sinc}(\mu)\equiv\sin(\mu)/\mu$. Thus, the far-field pressure (or similarly, the focal-plane pressure) obtained for any rectangularly symmetric aperture of the form given by Eq. (10) can be written in terms of the far-field pattern of a uniform, unfocused rectangular aperture, given appropriate scaling and shifting of wave number and azimuthal coordinates according to Eq. (12).

In a second limiting case, the pressure field due to an unfocused or focused Gaussian amplitude distribution takes the form of a Gaussian beam in the limit of an infinite aperture, so that $a\to\infty$ and $b\to\infty$. In this limit, the pressure field becomes the Gaussian beam

$$\begin{aligned} p(\mathbf{r}) &\to \frac{k}{\sqrt{\tilde{k}_x}\sqrt{\tilde{k}_y}}\Phi(\mathbf{r},\zeta) \\ &= -\frac{i\zeta}{k\tilde{\sigma}_x\tilde{\sigma}_y}e^{ik(r^2+\zeta^2)/(2\zeta)}e^{-x^2/(2\tilde{\sigma}_x^2)}e^{-y^2/(2\tilde{\sigma}_y^2)}, \end{aligned} \quad (21)$$

where

$$\begin{aligned} \tilde{\sigma}_x &\equiv \frac{\zeta\sqrt{1-ik\sigma_x^2(1/\zeta-1/F_x)}}{k\sigma_x}, \\ \tilde{\sigma}_y &\equiv \frac{\zeta\sqrt{1-ik\sigma_y^2(1/\zeta-1/F_y)}}{k\sigma_y}, \end{aligned} \quad (22)$$

and the scaled parameters $\tilde{k}_x$, $\tilde{k}_y$, $\tilde{x}$, and $\tilde{y}$ are those defined in Table II for the truncated Gaussian aperture. This is consistent with previous results showing that beams from Gaussian sources remain Gaussian in shape at all ranges.[25,38]

C. Error function aperture

One potential apodization design uses an essentially rectangular amplitude distribution, with tapered edges to reduce sidelobes.[11] A simple mathematical representation for such apertures is a Gaussian function convolved with a rectangle, resulting in an error function amplitude distribution. This representation has been successfully employed in modeling the nonuniform amplitude distribution of conventional, nominally nonapodized transducers, and can provide better agreement with experiment than uniform amplitude distributions.[39] The resulting apodization has an effect similar to the piecewise-continuous "step function with 'smooth' edge" introduced by Tjøtta and Tjøtta.[40] For the general case including focusing, the error-function velocity distribution can be written for the approximations considered here as

$$\begin{aligned} A_x(x_0) &= \frac{e^{-ikx_0^2/(2F_x)}}{\sqrt{2\pi}\sigma_x}\int_{-a}^{a}e^{-(x_1-x_0)^2/(2\sigma_x^2)}dx_1 \\ &= \frac{e^{-ikx_0^2/(2F_x)}}{2}\left(\mathrm{erf}\left[\frac{x_0+a}{\sqrt{2}\sigma_x}\right]-\mathrm{erf}\left[\frac{x_0-a}{\sqrt{2}\sigma_x}\right]\right) \end{aligned} \quad (23)$$

for the x direction, and similarly for the y direction in terms of F_y and σ_y, where σ_x and σ_y are nonzero real parameters that determine the sharpness of the aperture taper.

The pressure field defined by Eq. (9) can thus be written for the error function aperture as a product of double integrals,

$$\begin{aligned} p(\mathbf{r}) = -\frac{ike^{ik(r^2+\zeta^2)/(2\zeta)}}{4\pi^2\sigma_x\sigma_y\zeta}&\int_{-\infty}^{\infty}\int_{-a}^{a}e^{-(x_1-x_0)^2/(2\sigma_x^2)} \\ &\times e^{-ikx_0^2/(2F_x)}e^{ik(x_0^2-2xx_0)/(2\zeta)}dx_1dx_0 \\ &\times\int_{-\infty}^{\infty}\int_{-b}^{b}e^{-(y_1-y_0)^2/(2\sigma_y^2)} \\ &\times e^{-iky_0^2/(2F_y)}e^{ik(y_0^2-2yy_0)/(2\zeta)}dy_1dy_0. \end{aligned} \quad (24)$$

After some algebraic manipulation and exchanging the order of integration, this can be rewritten as

$$\begin{aligned} p(\mathbf{r}) = -\frac{ike^{ik(r^2+\zeta^2)/(2\zeta)}e^{-k^2(\sigma_x^2\tilde{x}x+\sigma_y^2\tilde{y}y)/(2\zeta^2)}}{4\pi^2\sigma_x\sigma_y\zeta}& \\ \times\int_{-a}^{a}\left[\int_{-\infty}^{\infty}e^{-(x_0-\chi_x)^2/(2\sigma_x^2\tilde{x}/x)}dx_0\right]e^{i(\tilde{k}_xx_1^2-2k\tilde{x}x_1)/(2\zeta)}dx_1& \\ \times\int_{-b}^{b}\left[\int_{-\infty}^{\infty}e^{-(y_0-\chi_y)^2/(2\sigma_y^2\tilde{y}/y)}dy_0\right]e^{i(\tilde{k}_yy_1^2-2k\tilde{y}y_1)/(2\zeta)}dy_1,& \end{aligned} \quad (25)$$

where

$$\begin{aligned} \tilde{k}_x &\equiv \frac{k(1-\zeta/F_x)}{1+ik\sigma_x^2(1/F_x-1/\zeta)}, \\ \tilde{x} &\equiv \frac{x}{1+ik\sigma_x^2(1/F_x-1/\zeta)}, \\ \chi_x &\equiv \frac{x+ix_1\zeta/(k\sigma_x^2)}{1-\zeta/F_x+i\zeta/(k\sigma_x^2)}, \end{aligned} \quad (26)$$

and $\tilde{k}_y$, $\tilde{y}$, and $\tilde{\chi}_y$ are similarly defined in terms of y, y_1, F_y, and σ_y.

The integral over x_0 from Eq. (25) has the value $\sqrt{2\pi}\sigma_x/\sqrt{x/\tilde{x}}$, while the integral over y_0 similarly has the value $\sqrt{2\pi}\sigma_y/\sqrt{y/\tilde{y}}$. Equation (25) thus takes a form that is similar, except for multiplicative terms outside the integrals, to the integral pressure field expression of Eq. (9). Thus, the field pressure for the focused error-function aperture is given, in analogy to Eq. (13), by

$$p(\mathbf{r}) = \frac{k\Phi_e(\mathbf{r},\zeta)}{4\sqrt{\tilde{k}_x}\sqrt{\tilde{k}_y}}\left(\operatorname{erf}\left[\frac{k\tilde{x}+\tilde{k}_x a}{\sqrt{2i}\sqrt{\tilde{k}_x\zeta}}\right]-\operatorname{erf}\left[\frac{k\tilde{x}-\tilde{k}_x a}{\sqrt{2i}\sqrt{\tilde{k}_x\zeta}}\right]\right)$$
$$\times\left(\operatorname{erf}\left[\frac{k\tilde{y}+\tilde{k}_y b}{\sqrt{2i}\sqrt{\tilde{k}_y\zeta}}\right]-\operatorname{erf}\left[\frac{k\tilde{y}-\tilde{k}_y b}{\sqrt{2i}\sqrt{\tilde{k}_y\zeta}}\right]\right)$$
$$=-\frac{ik\Phi_e(\mathbf{r},\zeta)}{2\sqrt{\tilde{k}_x}\sqrt{\tilde{k}_y}}\left(\mathbf{F}\left[\frac{k\tilde{x}+\tilde{k}_x a}{\sqrt{\pi}\sqrt{\tilde{k}_x\zeta}}\right]-\mathbf{F}\left[\frac{k\tilde{x}-\tilde{k}_x a}{\sqrt{\pi}\sqrt{\tilde{k}_x\zeta}}\right]\right)$$
$$\times\left(\mathbf{F}\left[\frac{k\tilde{y}+\tilde{k}_y b}{\sqrt{\pi}\sqrt{\tilde{k}_y\zeta}}\right]-\mathbf{F}\left[\frac{k\tilde{y}-\tilde{k}_y b}{\sqrt{\pi}\sqrt{\tilde{k}_y\zeta}}\right]\right), \quad (27)$$

where the multiplicative term $\Phi_e(\mathbf{r},\zeta)$ is defined as

$$\Phi_e(\mathbf{r},\zeta) = \frac{e^{i[k(r^2+\zeta^2)-k^2(\tilde{x}^2/\tilde{k}_x+\tilde{y}^2/\tilde{k}_y)+ik^2(\sigma_x^2\tilde{x}x+\sigma_y^2\tilde{y}y)/\zeta]/(2\zeta)}}{\sqrt{x/\tilde{x}}\sqrt{y/\tilde{y}}} \quad (28)$$

and $\tilde{k}_x$, $\tilde{k}_y$, $\tilde{x}$, and $\tilde{y}$ are defined by Eq. (26). For an error function aperture that is unfocused in one or both dimensions, the field pressure under the Fresnel approximation is given by Eqs. (27) and (28) with either or both of the focal lengths set to infinity, so that $F_x\to\infty$ or $F_y\to\infty$ in the definitions from Eq. (26).

Thus, the pressure field of a focused or unfocused error-function aperture is functionally similar to that for other rectangularly symmetric sources, except for different scaled wave number and azimuthal distance parameters and a position-dependent multiplicative term. In the limit $\sigma_x\to 0$, $\sigma_y\to 0$, Eq. (27) reduces to the pressure field of a similarly focused or unfocused, uniform rectangular source.

III. NUMERICAL RESULTS

Since the general field expressions described earlier are exact, closed-form solutions of the Rayleigh integral under the Fresnel approximation, their accuracy depends mainly on the validity of the Fresnel approximations employed. To characterize the accuracy of the Fresnel approximations derived here, the field expressions derived earlier were compared with the impulse response method for three unfocused, uniform rectangular sources with dimensions relevant to ultrasonic applications. Accuracy of these field expressions, as a function of the source geometry and field position, should be comparable in the case of more complicated, apodized and focused apertures, for which the impulse response method is not applicable in general.

The computations reported here employed a wave number $k=20$ rad/mm, corresponding to a wavelength of 0.31 mm and a frequency of 5 MHz for radiation into water. The three sources examined included a small element with half-widths $a=0.5$ mm and $b=0.25$ mm (surface area $3.2\lambda\times 1.6\lambda$), a linear array element with $a=5.0$ mm and $b=0.15$ mm (area $32\lambda\times 1\lambda$), and a rectangular source with $a=5.0$ mm and $b=2.5$ mm (area $32\lambda\times 16\lambda$). In each case, fields for unfocused rectangular apertures were computed using Eq. (13) with $\tilde{x}=x$, $\tilde{y}=y$, and $\tilde{k}_x=\tilde{k}_y=k$ for each for the four Fresnel approximations (4)–(7).

For comparison, fields were computed at the same points using direct numerical evaluation of the impulse-response integral for time-harmonic excitation. The form used was the pressure impulse response derived by McGough, in which numerical conditioning is improved by subtraction of singularities that appear in the usual impulse-response integral, resulting in greater accuracy at lower computational cost.[18] The resulting field can be written for any point in space as

$$p(\mathbf{r}) = I(|x+a|,|y+b|) + \operatorname{sgn}(|a|-|x|)I(|x-a|,|y+b|)$$
$$+\operatorname{sgn}(|b|-|y|)I(|x+a|,|y-b|)$$
$$+\operatorname{sgn}(|a|-|x|)\operatorname{sgn}(|b|-|y|)I(|x-a|,|y-b|), \quad (29)$$

where sign is the signum function and I is an integral term computed numerically, defined as

$$I(s,l) = -\frac{1}{2\pi}\left(s\int_0^l \frac{e^{ik\sqrt{z^2+\sigma^2+s^2}}-e^{ikx}}{\sigma^2+s^2}d\sigma\right.$$
$$\left.+l\int_0^s \frac{e^{ik\sqrt{z^2+\sigma^2+l^2}}-e^{ikx}}{\sigma^2+l^2}d\sigma\right). \quad (30)$$

Both the Fresnel approximation of Eq. (13) and the numerical solution of Eqs. (29) and (30) were implemented directly on a commercial software package (MATHEMATICA 5.2, Wolfram Research), using complex error function and numerical integration routines provided in that package. The computation time required, for MATHEMATICA 5.2 under Linux on an AMD Athlon 64 3000+ processor running at 1.8 GHz, averaged 1.7×10^{-3} s per point for the Fresnel approximations and 1.2×10^{-2} s per point for direct numerical evaluation of the impulse response integral. Since these computation times were obtained using direct implementation of the respective formulas in a high-level, interpreted software language designed for high numerical precision, either method can achieve significantly greater performance when optimized for speed. With the Fresnel approximations derived here, comparable computational efficiency will also be obtained for any aperture with apodization and focusing characteristics described by Eq. (10), including cases for which the impulse response method may not be tractable.

Validity of the Fresnel approximations considered here can be qualitatively depicted, as a function of spatial position and transducer geometry, by representative computed fields. Figure 2 shows fields computed with the impulse-response integral and the four Fresnel approximations over a plane spanning 30×30 mm^2 at a range of 10 mm, displayed with a 40 dB dynamic range. These field plots illustrate the nature of each Fresnel approximation, with patterns corresponding to diffracted spherically spreading waves ($\zeta=r$), diffracted plane waves ($\zeta=z$), or diffracted cylindrically spreading waves ($\zeta=w_x$ and $\zeta=w_y$).

In Fig. 2(a), illustrating the field of a small element, the Fresnel approximation based on diffracted spherical waves ($\zeta=r$) captures the detailed field features accurately, while the other Fresnel approximations poorly represent the field in this case. In Fig. 2(b), showing the field of a linear array element, the field is accurately depicted by the Fresnel approximations associated with diffracted spherically spreading

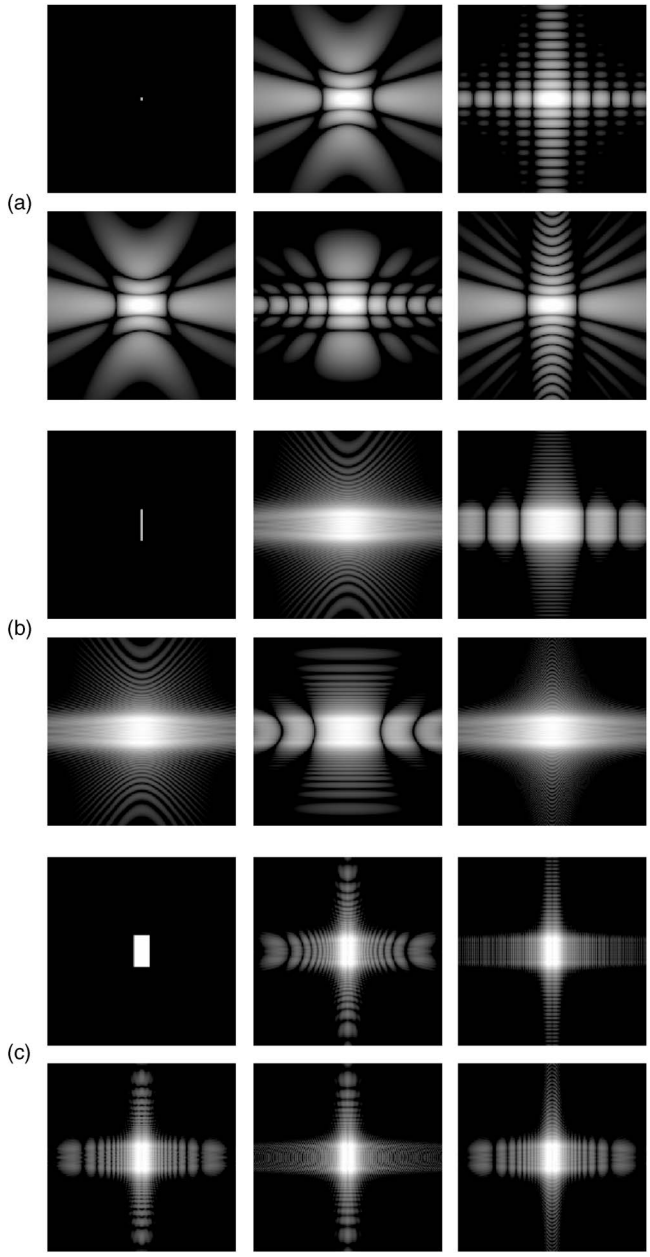

FIG. 2. Aperture velocity distributions and computed pressure fields at a range of 10 mm for three apertures with wave number $k=20$ rad/mm. Computed pressure magnitudes are shown on a logarithmic grayscale with 40 dB dynamic range. Each plot shows a region of size 30×30 mm^2. Top left: Aperture velocity distribution. Bottom left: Reference field from numerical solution of the impulse-response integral. Computed fields from the four Fresnel approximations considered are arranged with $\zeta=r$ (diffracted spherical wave) at top middle, $\zeta=z$ (diffracted plane wave) at top right, $\zeta=w_x$ (diffracted yz-plane cylindrical wave) at bottom middle, and $\zeta=w_y$ (diffracted xz-plane cylindrical wave) at bottom right. (a) $a=0.5$ mm, $b=0.25$ mm. (b) $a=5.0$ mm, $b=0.15$ mm. (c) $a=5.0$ mm, $b=2.5$ mm.

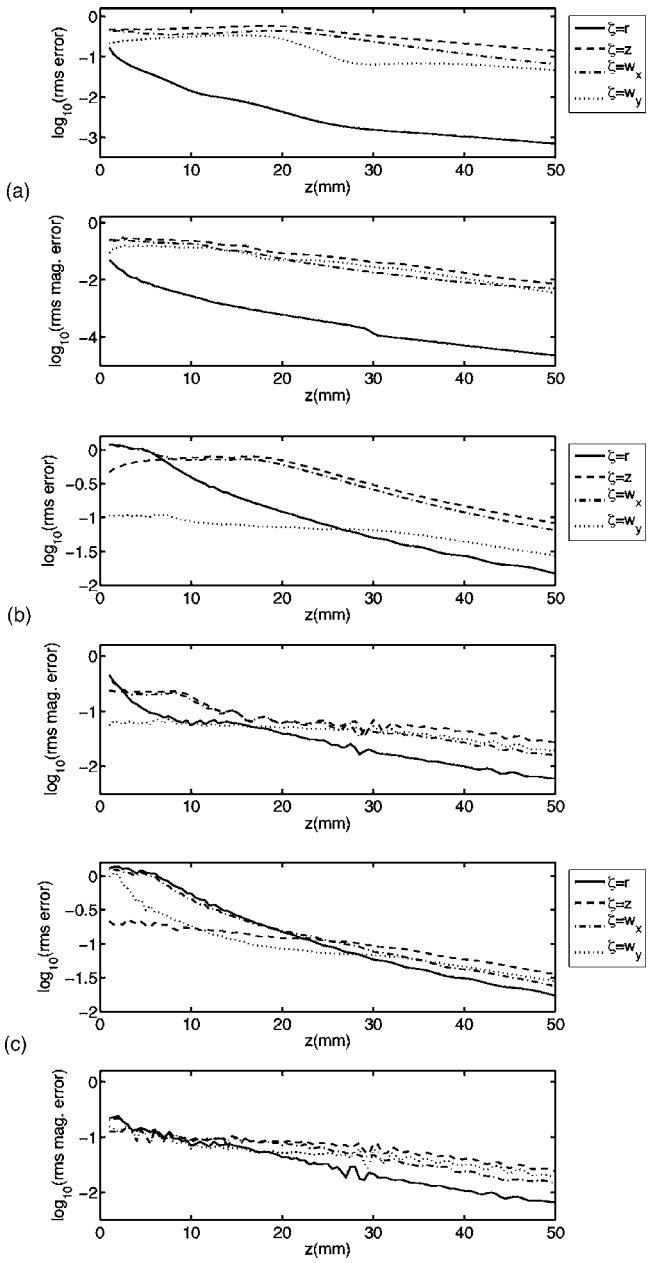

FIG. 3. Computed rms error for four Fresnel approximations and three aperture configurations, plotted as a function of range z for a wave number $k=20$ rad/mm. In each panel, logarithmic plots are shown for both the rms complex pressure error, $\langle|p-p_{\mathrm{refl}}|\rangle/\langle|p_{\mathrm{refl}}|\rangle$, and the rms pressure magnitude error, $\langle|p|-|p_{\mathrm{refl}}|\rangle\langle|p_{\mathrm{refl}}|\rangle$, as defined in Eqs. (31) and (32). (a) $a=0.5$ mm, $b=0.25$ mm. (b) $a=5.0$ mm, $b=0.15$ mm. (c) $a=5.0$ mm, $b=2.5$ mm.

waves ($\zeta=r$) and with diffracted cylindrically spreading waves around the element's long axis ($\zeta=w_x$), while the other Fresnel approximations are inaccurate for this source geometry. It may be noted that at this range, the $\zeta=r$ approximation more closely resembles the low-level detail of the linear-array element field, even though the $\zeta=w_x$ approximation achieves better overall quantitative accuracy, as shown in Fig. 3. Figure 2(c), which shows fields computed for a large rectangular element, shows that all four Fresnel approximations properly depict the collimated main beam. The low-level field details in this case are captured partially by each of the four Fresnel approximations. In all cases, the regions of greatest computational accuracy are consistent with those listed in Table I for each Fresnel approximation.

The quantitative accuracy achieved by each of the four Fresnel approximations is illustrated in Fig. 3 for the three source configurations shown in Fig. 2. In each case, fields were computed using the four Fresnel approximations over a three-dimensional region spanning from 0.2 to 50 mm in range (z) and 0–10 mm in the elevation and azimuthal di-

rections (x and y), with a spatial step size of 0.2 mm in each direction. The rms error for the complex pressure field in each z plane was defined as

$$\frac{\langle |p - p_{\text{ref}}| \rangle}{\langle |p_{\text{ref}}| \rangle} = \sqrt{\frac{\sum_x \sum_y |p(\mathbf{r}) - p_{\text{ref}}(\mathbf{r})|^2}{\sum_x \sum_y |p_{\text{ref}}(\mathbf{r})|^2}}, \tag{31}$$

where $p(\mathbf{r})$ is the complex pressure wave field computed using a Fresnel approximation and $p_{\text{ref}}(\mathbf{r})$ is the complex pressure wave field computed using direct numerical solution of the impulse-response integral. Similarly, the rms error for the pressure magnitude was defined as

$$\frac{\langle |p| - |p_{\text{ref}}| \rangle}{\langle |p_{\text{ref}}| \rangle} = \sqrt{\frac{\sum_x \sum_y (|p(\mathbf{r})| - |p_{\text{ref}}(\mathbf{r})|)^2}{\sum_x \sum_y |p_{\text{ref}}(\mathbf{r})|^2}}. \tag{32}$$

The error results shown in Fig. 3 illustrate how the applicability of each approximation varies depending on the source configuration as well as the range of interest. For the small source (a), the Fresnel approximation based on spherical spreading ($\zeta = r$) is the most accurate at all ranges. For the linear array element (b) and the larger rectangular source (c), the $\zeta = r$ approximation provides the most accurate results at larger ranges, but near the source more accurate results are obtained by the Fresnel approximation corresponding to the source geometry. For the linear array element (b), the diffracted cylindrical-wave approximation ($\zeta = w_x$) is the most accurate near the source, while for the rectangular source (c) the diffracted plane-wave approximation ($\zeta = z$) is the most accurate near the source.

In all cases, choice of the most appropriate approximation yields pressure fields with complex pressure errors on the order of 10% or less and magnitude errors of several percent, except for points very near the transducer surface. This performance is consistent with previous results demonstrating amplitude and phase errors of 1% to 2% for the Fresnel approximation applied to collimated beam propagation within the near field.[41] This level of accuracy is sufficient for many practical ultrasound applications. Comparable accuracy can be expected for other, more general source distributions of the form given by Eq. (10).

The Fresnel approximation methods described here provide simple analytic expressions for pressure fields from many aperture configurations, including various amplitude distributions and independent azimuthal and elevation focusing. These features are illustrated in Figs. 4–6, which illustrate the fields of 10×10 mm^2 rectangular apertures with uniform and error-function apodizations, focused at a distance of 20 mm in an attenuating medium. The wave number employed was $k = 20 + 0.0288i$ rad/mm, corresponding to a 5 MHz frequency for radiation into a water-like medium with a tissue-mimicking attenuation of 2.5 dB/cm. Figure 4 shows the on-axis pressure magnitude for the uniform, focused rectangular aperture case ($\sigma = 0$), computed both by the Fresnel approximation ($\zeta = r$) and by direct numerical evaluation of the Rayleigh integral [Eq. (1)], both with the quadratic focusing phase specified by Eq. (17). In the software package employed (MATHEMATICA 5.2, with the above-described computer configuration), the required computation time for this plot was 0.63 s for the Fresnel approximation and 3.7×10^3 s for direct evaluation of the Rayleigh integral. The Fresnel approximation predicts the peak position in this case with less than 3% error and the peak pressure magnitude with less than 2% error. Positions of local, diffraction-induced peaks and nulls are less accurate for small axial distances where the Fresnel approximation is less valid.

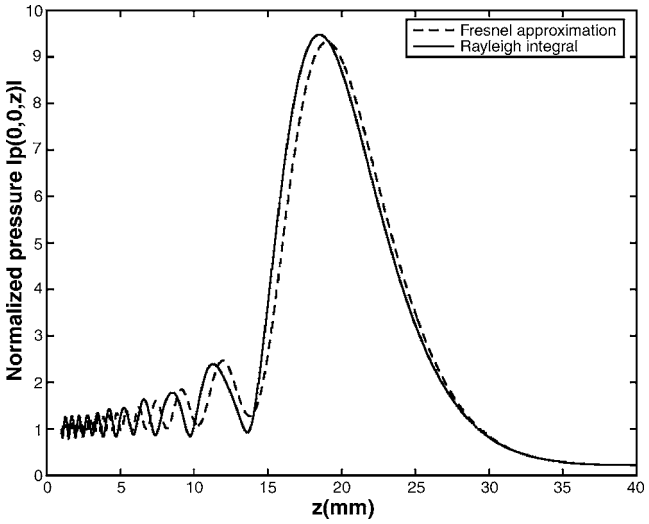

FIG. 4. On-axis pressure magnitudes, computed using the Fresnel approximation and numerical evaluation of the Rayleigh integral, for a 10×10 mm^2 aperture with a focal length of 20 mm in both the x and y directions and a wave number of $20 + 0.0288i$ rad/mm.

To illustrate use of the solutions presented here for computation of source apodization effects, the focused aperture configuration used for Fig. 4 can be compared to error-function apodized sources of the same dimensions. The four error function apodizations employed, ranging from no apodization ($\sigma = 0$ mm) to significant smoothing

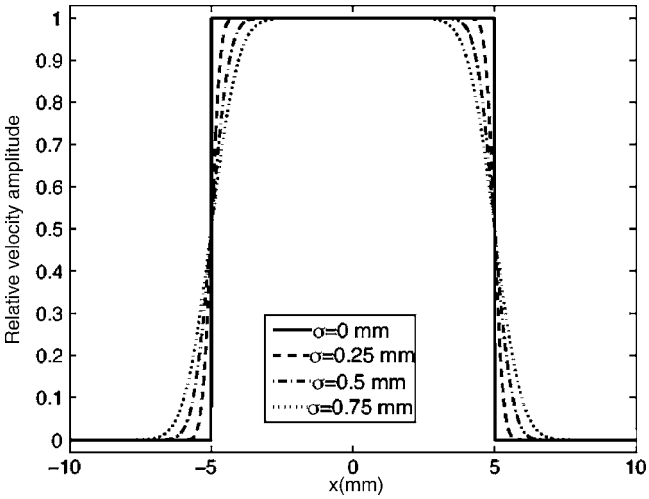

FIG. 5. Error function apodizations used in the test computation for a focused aperture. The parameter $\sigma = 0$ mm corresponds to a rectangular aperture while increasing σ results in greater smoothing of the source amplitude distribution.

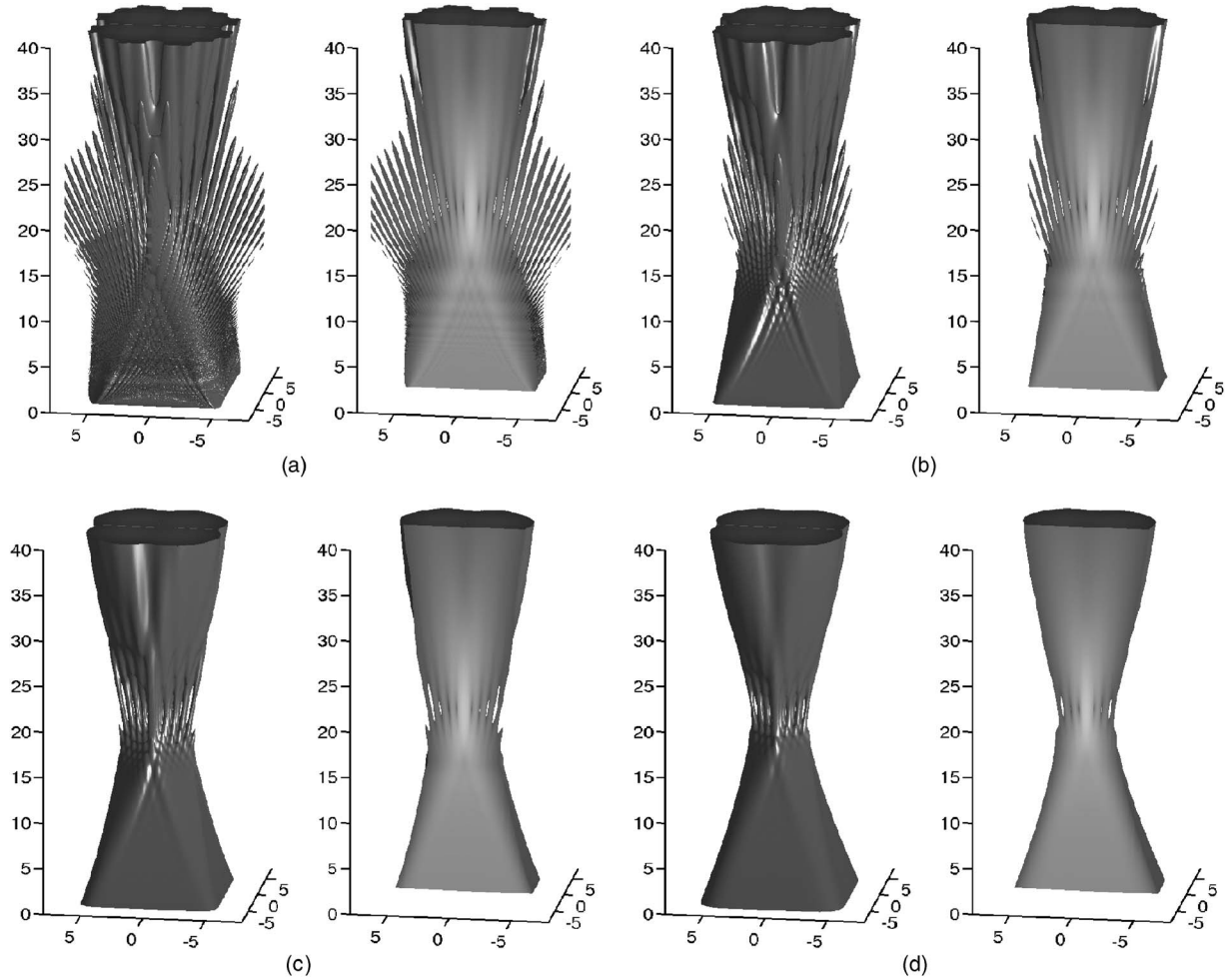

FIG. 6. Three-dimensional pressure fields for the four error function apodizations of Fig. 5, applied to a 10×10 mm^2 aperture with a focal length of 20 mm in both the x and y directions and a wave number of $20+0.0288i$ rad/mm. Each panel shows a rendering of the pressure magnitude isosurface at a level 36 dB below the peak (left) as well as the xz-plane pressure magnitude, logarithmically scaled and superimposed on a half-space −36 dB isosurface rendering (right).

($\sigma=0.75$ mm), are plotted in Fig. 5. Isosurface renderings and xz-plane cross sections of pressure magnitudes for the four apodization conditions, computed using Eq. (27) with $\zeta=z$, are displayed in Fig. 6. As the parameter σ increases, the rectangular aperture is increasingly smoothed, causing the sidelobes to fall markedly while the width of the main lobe remains essentially constant.

IV. DISCUSSION

The approximations described here should be useful for large-scale computations of radiated acoustic fields, as well as for further analytic studies. Several aspects concerning the practical application of these methods are discussed here.

A. Accuracy and efficiency of computations

As illustrated by Figs. 2 and 3, accuracy of computations can be affected by the choice of Fresnel approximation employed. The numerical results reported here suggest that the Fresnel approximation based on diffracted spherically spreading waves ($\zeta=r$) provides the most accurate results for a variety of source configurations, if the distance of interest is more than several source diameters from the center of the aperture. For distances less than several source diameters, the appropriate choice of approximation depends on the source configuration. For sources that are much longer in one dimension, the most appropriate Fresnel approximation near the source is based on diffracted cylindrical waves centered on the long axis of the source, e.g., $\zeta=w_x$ for the source configuration shown in Fig. 2(b). For sources that are large compared to the wavelength in two dimensions, the most appropriate Fresnel approximation near the source represents the field as a diffracted plane wave ($\zeta=z$).

The absolute accuracy achievable using the Fresnel approximations is good, with relative errors on the order of 10% near the source, and errors of less than 1% at distances large compared to the source dimensions. Thus, these approximations should be suitable for many ultrasound applications, including characterization of beam patterns for diffraction correction in scattering and attenuation measurements and simulation of ultrasound imaging methods. For simulation of ultrasound imaging methods,[4–7] accurate depiction of low-level detail in ultrasound beams may be particularly important, in which case the Fresnel approximation describing diffracted spherical waves ($\zeta=r$) may be most appropriate throughout the region of interest. The methods provide increased accuracy when only the pressure mag-

nitude is of interest, as is the case for many applications such as simulation of heating caused by therapeutic ultrasound arrays.[1–3]

The numerical efficiency of the Fresnel approximations shown here is excellent, although definitive optimization of computation speed is beyond the scope of the present paper. Since pressure fields for all the apertures considered have been expressed in closed form in terms of the error function and Fresnel integral, available methods for optimizing computation of these special functions[42,43] would further improve the efficiency of the pressure computations. For example, both the Fresnel integral and the complex error function can be evaluated accurately using rational approximations,[32,43] which can be used to compute these special functions using only a few arithmetic operations at each point.

B. Extension to other configurations

The methods described here provide explicit analytic formulas for the time-harmonic fields of rectangularly symmetric, unfocused or focused apertures with a variety of surface velocity distributions. These formulas can be employed to compute fields for more complex configurations including radiation from arrays of rectangularly symmetric elements and from pulsed sources.

Radiation from transducer arrays composed of rectangularly symmetric elements can be simulated by computing the field from each individual element in a coordinate system originating from the element center, and superposing the fields with the desired amplitude and phase weighting. This process has been described elsewhere[3,10] and has been shown to result in good agreement between computed and measured array fields.[44]

The Fresnel approximations described here are based on the frequency-domain Rayleigh integral, so that they are directly applicable to continuous-wave sources. Many ultrasound applications, such as modeling of ultrasound ablation,[1–3] continuous-wave imaging systems,[5] and analysis of scattering measurements,[8–10] require only computation of continuous-wave radiated fields. Fields of narrow-band (e.g., tone burst) sources can also be closely approximated by these single-frequency fields, using amplitude envelopes specified by the source wave form and the acoustic travel time to the field point.[45] Thus, for a source wave form

$$u(t) = w(t)e^{-i\omega t},$$

the time-domain pressure field is given approximately by

$$p(\mathbf{r},t) = \mathrm{Re}[p(\mathbf{r})w(t-\zeta/c)e^{-i\omega t}], \tag{33}$$

where $p(\mathbf{r})$ is a single-frequency pressure field as given by Eqs. (9), (13), or Eq. (27), and ζ is the nominal propagation distance for the Fresnel approximation employed (e.g., $\zeta=z$ for a diffracted plane wave, $\zeta=r$ for a diffracted spherical wave, and $\zeta=w_y$ or $\zeta=w_x$ for a diffracted cylindrical wave).

For wideband sources such as ultrasonic array elements excited by short pulses, time-domain pressure fields can be obtained from the approximations derived here by computing separate frequency components and performing an inverse temporal Fourier transform of the field at each spatial point. This process is most efficient for relatively narrow-band signals, for which the field can be accurately characterized using a small number of temporal frequency components.

V. CONCLUSION

This work has provided analytic expressions for the acoustic fields of a wide variety of baffled, rectangularly symmetric sources, including focused and unfocused apertures with various forms of amplitude apodization. All of these analytic expressions can be expressed in a form similar to the previously derived field of an unfocused rectangular piston, and are valid for several different instances of the Fresnel approximation. Given the choice of the Fresnel approximation most suited to the source geometry and field region of interest, the analytically determined fields accurately approximate the true radiated fields, allowing both field computations and further analytic study of radiation from rectangularly symmetric sources.

[1] C. Lafon, F. Prat, J. Y. Chapelon, F. Gorry, J. Margonari, Y. Theillere, and D. Cathignol, "Cylindrical thermal coagulation necrosis using an interstitial applicator with a plane ultrasonic transducer: *in vitro* and *in vivo* experiments versus computer simulations," Int. J. Hyperthermia **16**, 508–522 (2000).

[2] R. Chopra, M. J. Bronskill, and F. S. Foster, "Feasibility of linear arrays for interstitial ultrasound thermal therapy," Med. Phys. **27**, 1281–1286 (2000).

[3] T. D. Mast, I. R. S. Makin, W. Faidi, M. M. Runk, P. G. Barthe, and M. H. Slayton, "Bulk ablation of soft tissue with intense ultrasound: Modeling and experiments," J. Acoust. Soc. Am. **118**, 2715–2724 (2005).

[4] Y. Li and J. A. Zagzebski, "A frequency domain model for generating B-mode images with array transducers," IEEE Trans. Ultrason. Ferroelectr. Freq. Control **46**, 690–699 (1999).

[5] T. Jansson, T. D. Mast, H. W. Persson, and K. Lindström, "Frequency dependence of speckle in continuous-wave ultrasound with implications for blood perfusion measurements," IEEE Trans. Ultrason. Ferroelectr. Freq. Control **49**, 715–725 (2002).

[6] J. A. Jensen, "Simulation of advanced ultrasound systems using Field II," Proceedings of the 2004 IEEE International Symposium on Biomedical Imaging, Arlington, VA, April 2004, pp. 636–639.

[7] Y.-T. Shen and J. C. Lacefield, "First-order speckle statistics of ultrasound breast images synthesized from a computational anatomy model," Can. Acoust. **33**, 86–87 (2005).

[8] M. F. Insana, T. J. Hall, and L. T. Cook, "Backscatter coefficient estimation using array transducers," IEEE Trans. Ultrason. Ferroelectr. Freq. Control **41**, 714–723 (1994).

[9] X. Chen, D. Phillips, K. Q. Schwarz, J. G. Mottley, and K. J. Parker, "The measurement of backscatter coefficient from a broadband pulse-echo system: A new formulation," IEEE Trans. Ultrason. Ferroelectr. Freq. Control **44**, 515–525 (1997).

[10] T. T. Jansson, T. D. Mast, and R. C. Waag, "Measurements of differential scattering cross-section using a ring transducer," J. Acoust. Soc. Am. **103**, 3169–3179 (1998).

[11] T. L. Szabo, *Diagnostic Ultrasound Imaging: Inside Out* (Elsevier, Burlington, MA, 2004), Chap. 6.

[12] P. R. Stepanishen and K. C. Benjamin, "Forward and backward projection of acoustic fields using FFT methods," J. Acoust. Soc. Am. **71**, 803–812 (1982).

[13] E. G. Williams and J. D. Maynard, "Numerical evaluation of the Rayleigh integral for planar radiators using the FFT," J. Acoust. Soc. Am. **72**, 2020–2030 (1982).

[14] P. R. Stepanishen, "The time-dependent force and radiation impedance on a piston in a rigid infinite planar baffle," J. Acoust. Soc. Am. **49**, 841–849 (1971).

[15] J. C. Lockwood and J. G. Willette, "High-speed method for computing the exact solution for the pressure variations in the nearfield of a baffled piston," J. Acoust. Soc. Am. **53**, 735–741 (1973).

[16] J. L. San Emeterio and L. G. Ullate, "Diffraction impulse-response of rectangular transducers," J. Acoust. Soc. Am. **92**, 651–662 (1992).

[17]A. Neild and D. A. Hutchins, "A theoretical model for a finite-size acoustic receiver," J. Acoust. Soc. Am. **155**, 1546–1556 (2004).
[18]R. J. McGough, "Rapid calculations of time-harmonic nearfield pressures produced by rectangular pistons," J. Acoust. Soc. Am. **115**, 1934–1941 (2004).
[19]P. Faure, D. Cathignol, and J. Y. Chapelon, "On the pressure field of a transducer in the form of a curved strip," J. Acoust. Soc. Am. **95**, 628–637 (1994).
[20]K. B. Ocheltree and L. A. Frizzell, "Sound field calculation for rectangular sources," IEEE Trans. Ultrason. Ferroelectr. Freq. Control **46**, 242–248 (1989).
[21]C. Lee and P. J. Benkeser, "A computationally efficient method for the calculation of the transient field of acoustic radiators," J. Acoust. Soc. Am. **96**, 545–551 (1994).
[22]B. Ü. Karbeyaz, E. L. Miller, and R. O. Cleveland, "Semi-analytical computation of the acoustic field of a segment of a cylindrically concave transducer in lossless and attenuating media," J. Acoust. Soc. Am. **121**, 1226–1237 (2007).
[23]J. W. Goodman, *Introduction to Fourier Optics*, 3rd ed. (Roberts & Co., Greenwood Village, CO, 2005), Chap. 4.
[24]A. Freedman, "Sound field of a rectangular piston," J. Acoust. Soc. Am. **32**, 197–209 (1960).
[25]T. L. Szabo, "Generalized Fourier transform diffraction theory for parabolically anisotropic media," J. Acoust. Soc. Am. **63**, 28–34 (1978).
[26]D. Ding,Y. Zhang, and J. Liu, "Some extensions of the Gaussian beam expansion: Radiation fields of the rectangular and the elliptical transducer," J. Acoust. Soc. Am. **113**, 3043–3048 (2003).
[27]B. D. Cook and W. J. Arnoult III, "Gaussian-Laguerre/Hermite formula for the nearfield of an ultrasonic transducer," J. Acoust. Soc. Am. **59**, 9–11 (1976).
[28]J. J. Wen and M. A. Breazeale, "A diffraction beam field expressed as the superposition of Gaussian beams," J. Acoust. Soc. Am. **83**, 1752–1756 (1988).
[29]A. Sahin and A. C. Baker, "Ultrasonic pressure fields due to rectangular apertures," J. Acoust. Soc. Am. **96**, 552–556 (1994).
[30]K. Sha, J. Yang, and W.-S. Gan, "A complex virtual source approach for calculating the diffraction beam field generated by a rectangular planar source," IEEE Trans. Ultrason. Ferroelectr. Freq. Control **50**, 890–897 (2003).
[31]A. D. Pierce, *Acoustics: An Introduction to its Physical Principles and Applications*, 2nd ed. (Acoustical Society of America, Melville, NY, 1989), Chap. 5.
[32]M. Abramowitz and I. A. Stegun, *Handbook of Mathematical Functions* (National Bureau of Standards, Washington, DC, 1972), Chap. 7.
[33]S. Zhang and J. Jin, *Computation of Special Functions* (Wiley, New York, 1996), Chap. 16.
[34]S. Wolfram, *The Mathematica Book*, 4th ed. (Cambridge University Press, New York, 1999), pp. 766, 1125, 1143.
[35]T. D. Mast and F. Yu, "Simplified expansions for radiation from a baffled circular piston," J. Acoust. Soc. Am. **118**, 3457–3464 (2005).
[36]N. F. Declercq and J. Degneck, "The Laplace transform to describe bounded inhomogeneous waves," J. Acoust. Soc. Am. **116**, 51–60 (2004).
[37]M. Greenspan, "Piston radiator: Some extensions of the theory," J. Acoust. Soc. Am. **65**, 608–621 (1979).
[38]I. M. Mason, "Anisotropy, diffraction scaling, surface wave lenses, and focusing," J. Acoust. Soc. Am. **53**, 1123–1128 (1973).
[39]T. Lawu, M. Tabei, and M. Ueda, "Near-field ultrasonic scattering from a cavity in steel considering the velocity amplitude on the transducer face using an error function model," J. Acoust. Soc. Am. **104**, 1242–1245 (1998).
[40]J. Naze Tjøtta and S. Tjøtta, "Nearfield and farfield of pulsed acoustic radiators," J. Acoust. Soc. Am. **118**, 3457–3464 (2005).
[41]W. H. Southwell, "Validity of the Fresnel approximation in the near field," J. Opt. Soc. Am. **71**, 7–14 (1998).
[42]G. Poppe and C. Wijers, "More efficient computation of the complex error function," ACM Trans. Math. Softw. **16**, 38–46 (1990).
[43]J. A. C. Weideman, "Computation of the complex error function," SIAM (Soc. Ind. Appl. Math.) J. Numer. Anal. **31**, 1497–1518 (1994).
[44]I. R. S. Makin, T. D. Mast, W. Faidi, M. M. Runk, P. G. Barthe, and M. H. Slayton, "Miniaturized ultrasound arrays for interstitial ablation and imaging," Ultrasound Med. Biol. **31**, 1539–1550 (2005).
[45]J. A. Campbell and R. C. Waag, "Normalization of ultrasonic scattering measurements to obtain average differential scattering cross sections for tissues," J. Acoust. Soc. Am. **74**, 393–399 (1983).